Cancer Research

PET Imaging of Tumor Neovascularization in a Transgenic Mouse Model with a Novel ^{64}Cu-DOTA-Knottin Peptide

Carsten H. Nielsen[1,5], Richard H. Kimura[1], Nadia Withofs[1], Phuoc T. Tran[3,4], Zheng Miao[1], Jennifer R. Cochran[2], Zhen Cheng[1], Dean Felsher[3], Andreas Kjær[5], Juergen K. Willmann[1], and Sanjiv S. Gambhir[1,2]

Abstract

Due to the high mortality of lung cancer, there is a critical need to develop diagnostic procedures enabling early detection of the disease while at a curable stage. Targeted molecular imaging builds on the positive attributes of positron emission tomography/computed tomography (PET/CT) to allow for a noninvasive detection and characterization of smaller lung nodules, thus increasing the chances of positive treatment outcome. In this study, we investigate the ability to characterize lung tumors that spontaneously arise in a transgenic mouse model. The tumors are first identified with small animal CT followed by characterization with the use of small animal PET with a novel ^{64}Cu–1,4,7,10-tetra-azacylododecane-N,N',N'',N'''-tetraacetic acid (DOTA)–knottin peptide that targets integrins upregulated during angiogenesis on the tumor associated neovasculature. The imaging results obtained with the knottin peptide are compared with standard ^{18}F-fluorodeoxyglucose (FDG) PET small animal imaging. Lung nodules as small as 3 mm in diameter were successfully identified in the transgenic mice by small animal CT, and both ^{64}Cu-DOTA-knottin 2.5F and FDG were able to differentiate lung nodules from the surrounding tissues. Uptake and retention of the ^{64}Cu-DOTA-knottin 2.5F tracer in the lung tumors combined with a low background in the thorax resulted in a statistically higher tumor to background (normal lung) ratio compared with FDG (6.01 ± 0.61 versus 4.36 ± 0.68; $P < 0.05$). *Ex vivo* biodistribution showed ^{64}Cu-DOTA-knottin 2.5F to have a fast renal clearance combined with low nonspecific accumulation in the thorax. Collectively, these results show ^{64}Cu-DOTA-knottin 2.5F to be a promising candidate for clinical translation for earlier detection and improved characterization of lung cancer. *Cancer Res; 70(22); 9022–30. ©2010 AACR.*

Introduction

Despite advances in cancer management and treatment, the mortality due to lung cancer is still strikingly high with an average 5-year survival of only 15% (1). The major contributor to the high mortality is diagnosis at a stage when the likelihood of effective treatment is low (2–4). Therefore, there is a need to develop technologies that will aid in the earlier detection of lung nodules (e.g., molecular imaging probes that are able to detect small tumors early in disease).

Low-dose computed tomography (CT) is increasingly utilized for screening patients with a high risk of developing lung cancer. CT screening has a high sensitivity (median, 96%; range, 81-100%; ref. 5) and can detect lung lesions in the subcentimeter range but is limited by a relatively low specificity (median, 82%; range, 50-95%; ref. 5), resulting in frequent false-positive screening results (5, 6). Combined positron emission tomography (PET) and CT with ^{18}fluorodeoxyglucose (FDG) can differentiate benign from malignant lesions >1 cm in diameter with high sensitivity and reasonably good specificity (6–8). However, noninvasive characterization of smaller lesions with ^{18}FDG-PET/CT remains challenging due to the low volume of tumor, the partial volume effect, and inherent background from metabolic active tissues in the region of interest. Invasive procedures, such as thin-needle biopsy, are difficult to do because of the small lesion size and number of potential lesions to biopsy, and challenging due to the associated high risk of missed sampling (7, 9–12). As clinical PET/CT scanners continue to improve in spatial resolution and sensitivity, there is an opportunity to improve tumor detection/management with better tracers. A targeted imaging modality offers the opportunity to expand on the positive attributes of PET/CT and allows for a noninvasive detection and characterization of smaller lung nodules, thus increasing the chances of positive treatment outcome.

Once a tumor grows beyond 1 to 2 mm in diameter, it becomes dependent on angiogenesis to support its growth (13, 14). Imaging probes that target cell surface markers

Authors' Affiliations: [1]Molecular Imaging Program at Stanford, Departments of Radiology and [2]Bioengineering, [3]Division of Oncology, Departments of Medicine and Pathology, and [4]Department of Radiation Oncology, Stanford University, Stanford, California; and [5]Cluster for Molecular Imaging and Department of Clinical Physiology, Nuclear Medicine and PET, Rigshospitalet, University of Copenhagen, Copenhagen, Denmark

Note: Supplementary data for this article are available at Cancer Research Online (http://cancerres.aacrjournals.org/).

Corresponding Author: Sanjiv Sam Gambhir, Molecular Imaging Program at Stanford, The James H. Clark Center, 1st Floor, East Wing, 318 Campus Drive, Stanford, CA 94305-5427. Phone: 650-725-2309; Fax: 650-724-4948; E-mail: sgambhir@stanford.edu.

doi: 10.1158/0008-5472.CAN-10-1338

related to angiogenesis, such as integrins, show potential for early cancer detection (15, 16). Integrins are a family of transmembrane-bound receptors consisting of α and β subunits noncovalently linked as heterodimers. Integrins are involved in cell-to-cell and cell-to-extracellular matrix adhesion, and play a major role in cell migration processes, such as angiogenesis and metastasis. Expression of integrins, particularly, $\alpha_v\beta_3$, $\alpha_v\beta_5$, and $\alpha_5\beta_1$, are significantly upregulated on tumor neovasculature and many tumor cells compared with quiescent endothelium and normal tissue (14–17), making them a promising target for differentiating tumor from normal vasculature.

In this study, we investigated the ability to image and characterize lung tumors that spontaneously arise in a transgenic mouse model. The tumors were first identified with small animal CT followed by characterization with the use of small animal PET with our novel ^{64}Cu–1,4,7,10-tetra-azacylododecane-N,N',N'',N'''-tetraacetic acid (DOTA)–knottin peptide engineered to bind integrin receptors with high affinity. Knottins, also known as cystine knots, are 20 to 60 amino acid peptides that consist of at least three interwoven disulfide bonds, imparting high thermal and proteolytic stability (18). Previously, we used the *Ecballium elaterium* trypsin inhibitor II (EETI-II), a knottin from the squash family of protease inhibitors, as a molecular scaffold to engineer peptides that bind with high affinity to tumor-related integrin receptors (17). We showed that the EETI-II–based knottin peptide 2.5F, which contains an Arg-Gly-Asp (RGD) motif, binds a range of integrins subtypes ($\alpha_v\beta_3$, $\alpha_v\beta_5$, and $\alpha_5\beta_1$) with affinities in the low nmol/L range and developed it as a promising new probe for molecular imaging applications in living subjects (19).

The conditional transgenic mouse model used in this study spontaneously develops lung tumors upon activation of the *K-Ras* and *MYC* oncogenes upon the administration of doxycycline (20). Lung tumor status was serially monitored by small animal CT screening, and mice with CT-positive lung lesions were further examined with the use of small animal PET. Comparative PET imaging was done with ^{64}Cu-DOTA-knottin 2.5F and ^{18}F-FDG (Fig. 1). Both probes were able to identify lung tumors seen on CT. Uptake and retention of the ^{64}Cu-DOTA-knottin 2.5F tracer in the lung tumor combined with a low background in the thorax resulted in a statistically higher tumor to background (normal lung) ratio compared with FDG, which shows the potential of ^{64}Cu-DOTA-knottin 2.5F to be a promising candidate for clinical translation for earlier detection and improved characterization of lung cancer.

Materials and Methods

Transgenic mouse model

A detailed description of the generation of the transgenic mouse model and genotyping by PCR has been previously

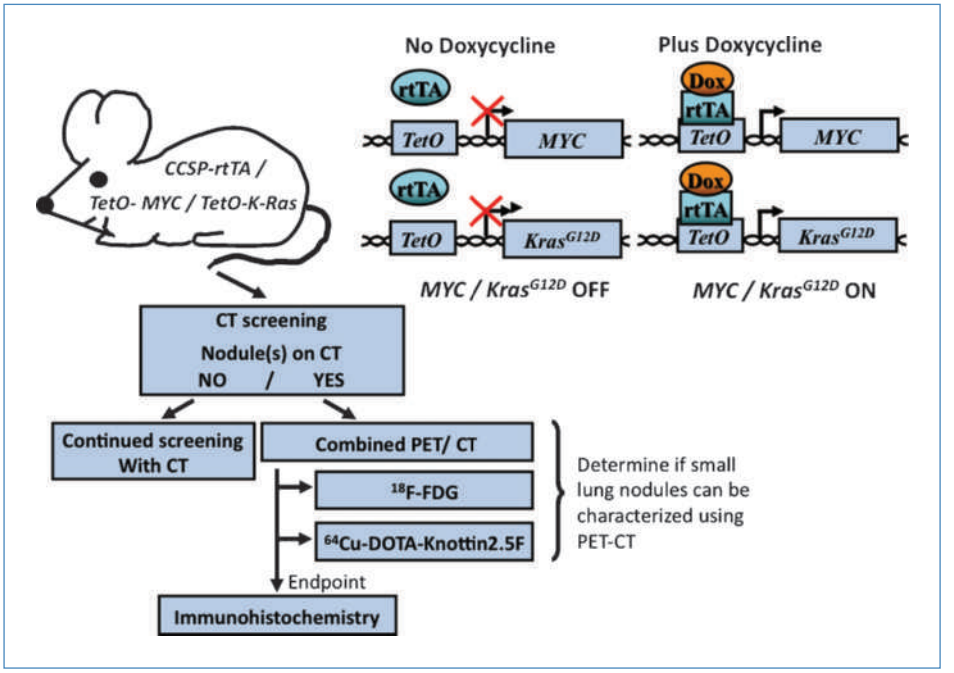

Figure 1. Schematic representation of experimental design. In the lung-specific conditional transgenic mouse model used in the study, expression of the rtTa is driven by the lung-specific *CCSP* promoter, and the expression of the oncogenes *Kras*^{G12D} and *MYC* is under control of the *TetO*. Absence of doxycycline prevents rtTA from binding to *TetO*; thus, there is no expression of *Kras*^{G12D} and *MYC*. Presence of doxycycline triggers a conformational change of *TetO* that enables rtTa binding, and expression of *Kras*^{G12D} and *MYC*. Expression of *Kras*^{G12D} and *MYC* is controlled by giving doxycyline through the drinking water. Lung tumors develop with an average latency of 36 weeks after administration of doxycycline (20). Serial small animal CT screening was used to monitor tumor development. Mice with positive CT findings underwent combined PET/CT with ^{18}F-FDG at day 0 and ^{64}Cu-DOTA-knottin 2.5F on day 1. Mice were sacrificed after imaging with ^{64}Cu-DOTA-knottin 2.5F (end point), and tumor sections were flash-frozen for immunofluorescence staining.

described (20, 21). Briefly, the transgenic mouse model used in the study was established by crossing transgenic lines containing the *Clara cell secretory protein* (*CCSP*) promoter driving the reverse tetracycline transactivating protein (rtTA), a *MYC* line under the control of the *tetracycline-responsive operon (TetO)* and a mutant $Kras^{G12D}$ line under control of *TetO*. The desired result was the biconditional model *CCSP-rtTa/TetO–MYC/TetO- Kras*^{G12D}.

Expression of the *MYC* and $Kras^{G12D}$ oncogenes was activated by weekly administration of 100 mg/mL doxycycline (Sigma) to the drinking water. Activation was initiated after weaning, typically 4 to 6 weeks of age, and tumors developed with an average latency of 36 weeks. All animal procedures were carried out according to a protocol approved by the Stanford University Administrative Panels on Laboratory Animal Care.

Small animal CT

Small animal CT scans were done with the use of a custom GE Medical Systems eXplore RS MicroCT System cone-beam scanner (GE Medical Systems). Seven transgenic mice with activated *MYC* and $Kras^{G12D}$ underwent serial small animal CT screening weekly for 3 weeks. Mice were anesthetized with 2% isofluorane in 2 L/min oxygen and positioned prone. Images were acquired at 97 μm resolution with a 70 kV (40 μA) beam, 12 ms exposure, and 400 radial views over a 360-degree rotation. The respiration was monitored during the scan with a BioVet monitoring system (m2m Imaging Corp.) and the acquisitions triggered to the end of the inspiratory phase.

Radiotracers

Synthesis and radiolabeling of the knottin 2.5F probe was done as previously described by us (19). ^{18}F-FDG was supplied by the cyclotron and radiochemistry facility at Stanford University with high specific activity.

Stability of ^{64}Cu-DOTA-knottin 2.5F

^{64}Cu-DOTA-knottin 2.5F in PBS was incubated in an equal volume of mouse serum at 37°C and analyzed at 1 and 4 hours after incubation. At the indicated time points, one volume of solvent A (99.9% H_2O and 0.1% trifluoroacetic acid) and one volume of dimethylformamide (Sigma) were added, and the resulting solution was centrifuged and filtered with a 0.2-micron spin filter (Corning). This mixture was analyzed by radio high-performance liquid chromatography (HPLC). Urine samples collected from mice 1 hour post-injection of ^{64}Cu-DOTA-knottin 2.5F was diluted to 1 mL with solvent A and analyzed by radio HPLC.

Ex vivo biodistribution

Healthy mice ($N = 5$) were anesthetized and injected with 66.3 to 70.6 μCi (2.45-2.61 MBq) of ^{64}Cu-DOTA-knottin 2.5F in 150 μL PBS through the tail vein and were euthanized 1 hour post-injection. The urine from 3 mice was collected for metabolite analysis by radio HPLC. Blood, heart, liver, lungs, muscle kidneys, spleen, brain, intestine, stomach, pancreas, and bone were removed and weighed. The radioactivity of each organ was measured by gamma counting and the activity level expressed as percent-injected dose/g tissue (%ID/g) or percent-injected dose/cm^3 (%ID/cm^3) for soft tissue and the lungs. Soft tissue was assumed to have a density of 1 g/cm^3. Before injection of the tracer, the mice ($N = 5$) underwent small animal CT. The densities of the lungs were calculated by dividing the weight of the lungs with the volumes estimated by CT.

Small animal PET/CT

A R4 microPET (Siemens Medical Solutions USA, Inc.) was used for small animal PET imaging. Mice with CT-positive nodules underwent PET imaging with ^{18}F-FDG on day 0 (relative to CT scan) and with ^{64}Cu-DOTA-knottin 2.5F on day 1. Mice were anesthetized with 2% isofluorane in 2 L/min oxygen and injected with 93 to 115 μCi (3.44-4.26 MBq) of either ^{18}F-FDG or ^{64}Cu-DOTA-knottin 2.5F in 150 μL PBS through the tail vein. Mice were placed in a holder with four fiducial markers, each containing ~0.5 μCi of either ^{18}F-FDG or ^{64}Cu-DOTA-knottin 2.5F in 10 μL iodine solution (30 mg/mL). Before the PET scan mice underwent small animal CT scanning as described above, followed by a 15-minute prone PET acquisition ~60 minutes post-injection of tracer. For ^{18}F-FDG-PET, mice were maintained under anesthesia in between injection and imaging. During anesthesia mice were kept warm on a heating pad. For knottin 2.5F, mice were allowed to recover from anesthesia in between injection and scanning. PET images were reconstructed with the use of the two-dimensional ordered subsets expectation maximization algorithm with a spatial resolution of 1.66 to 1.85 mm (22). No attenuation correction or partial volume corrections were applied.

Data analysis

All imaging data were analyzed offline with the use of software developed in our laboratory (AMIDE version 0.8.22; ref. 23), and the 3D volume viewer and analysis software (MicroView). Small animal PET/CT images were coregistered by manually identifying the center of the fiducial markers in the CT and PET images, and applying a built-in function for coregistration in the software. Regions of interest (ROIs) were subsequently drawn over the nodules and healthy lung tissue based on the CT images. Voxel values were converted to μCi/cm^3 by multiplying with a cylindrical factor obtained by scanning a cylindrical phantom with a known concentration of activity. For each ROI, the mean uptake as %ID/g was calculated assuming a tissue density of 1 g/cm^3. For each nodule the tumor-to-background ratio was calculated. The volumes of the lungs were estimated by drawing a rough ROI over the thorax of the mouse followed by simple binning to include only voxels with CT values corresponding to lung tissue.

Immunofluorescence

A subset of the mice ($N = 4$) were sacrificed immediately after ^{64}Cu-DOTA-knottin 2.5F PET imaging. The lungs were removed and dissected into pieces containing tumor tissue and lung tissue without visible tumor mass. The tissue pieces were embedded in optimal cutting temperature compound and flash frozen on dry ice. Frozen blocks were sectioned at 10 microns and mounted on charged glass slides for

immunofluorescence. A double-staining procedure was applied to visualize endothelial cells (CD31) and integrins (α_v-subunit). The following were used to stain for CD31: a rat anti-mouse CD31 primary antibody diluted 1:100 (BD Biosciences), a goat anti-rat biotinylated secondary antibody diluted 1:500 (Jackson ImmunoResearch Laboratories), and streptavidin-conjugated Alexa Fluor 488 diluted 1:200 (Invitrogen). The following were used to stain for α_v: a rat anti-mouse α_v-biotinylated primary antibody diluted 1:200 (Jackson ImmunoResearch Laboratories) and streptavidin-conjugated Alexa Fluor 594 diluted 1:200 (Invitrogen). Fluorescent images were acquired with a microscope (Axiophot, Carl Zeiss).

Statistical analysis

Data are given as mean ± SEM unless stated otherwise. The difference between the knottin 2.5F and FDG tumor-to-background ratios was assessed with the use of the two-sided Mann-Whitney test. A *P*-value <0.05 was considered statistically significant.

Results

Small animal CT screening

All seven transgenic mice that underwent serial small animal CT screening for 3 weeks were identified to have positive CT lung lesions. Next, we investigated the stability and biodistribution of the ^{64}Cu-DOTA-knottin 2.5F tracer before using it in a comparative study to characterize the lung lesions with the use of FDG and ^{64}Cu-DOTA-knottin 2.5F PET.

Serum and *in vivo* stability of knottin 2.5F

^{64}Cu-DOTA-knottin 2.5F incubated in mouse serum and urine samples from mice injected with ^{64}Cu-DOTA-knottin 2.5F were analyzed by radio HPLC to test the stability of the probe under physiologically relevant environments. All samples show a major elution peak at 14 minutes corresponding to the intact probe. The probe is mainly excreted intact in urine, and it is highly stable after 4 hours of serum incubation (Supplementary Fig. S1). Overall, the radio-HPLC analysis showed that the probe is stable at the conditions tested and is suitable as an *in vivo* imaging probe.

Ex vivo biodistribution

The biodistribution of ^{64}Cu-DOTA-knottin 2.5F was investigated in healthy mice 1 hour post-injection (Fig. 2). The tracer cleared rapidly through the kidneys (11.43 ± 1.45%ID/cm^3). Modest levels of background activity were observed in the stomach, intestine, spleen, and liver (1.28-2.53%ID/cm^3) in agreement with previous reports (19). Lower background signal was seen in the brain, blood, muscle, pancreas, lungs, and heart (0.04-0.50%ID/cm^3).

Small animal PET/CT

Mice with CT-positive tumors underwent PET imaging with ^{18}F-FDG and with ^{64}Cu-DOTA-knottin 2.5F. For both tracers, differentiation of lung nodules from surrounding lung tissue was possible based on PET images obtained 1 hour post-injection. However, in a few cases (N = 3), in which the nodules were in close proximity to the heart, delineation of nodule boundaries was very difficult with FDG-PET. This was due to relatively high ^{18}F-FDG uptake in the heart (26.92 ± 2.74%ID/g), leading to a spillover effect into the surrounding tissue. Importantly however, nodules that were obscured by high ^{18}F-FDG heart spillover were clearly visible on the ^{64}Cu-DOTA-knottin 2.5F images (Fig. 3). These images were made possible because of the low thoracic background signal that is characteristic of knottin peptides [18].

Overall, the radioactivity uptake in the nodules, measured as %ID/g by ROI analysis, was higher for ^{18}F-FDG compared with ^{64}Cu-DOTA-knottin 2.5F (Supplementary Fig. S2). However, ROI analysis of 10 distinguishable tumors showed a higher tumor-to-background ratio for the ^{64}Cu-DOTA-knottin 2.5F tracer compared with FDG (Table 1). The tumor-to-background ratio was 6.01 ± 0.61 (range, 3.51-9.05) for ^{64}Cu-DOTA-knottin 2.5F, which was significantly higher than the ratio obtained with FDG, 4.36 ± 0.68 (range, 1.70-8.30;

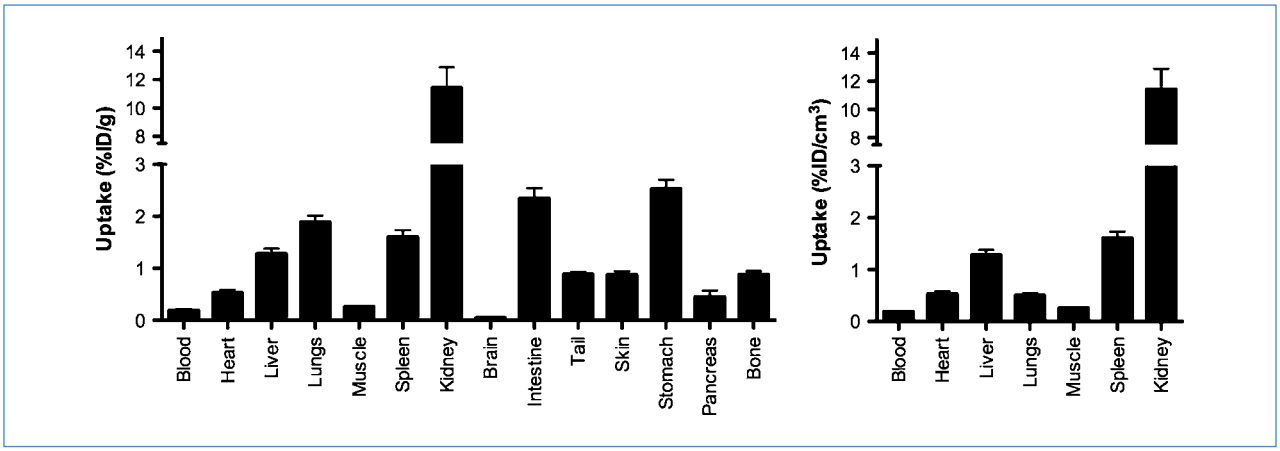

Figure 2. *Ex vivo* biodistribution of ^{64}Cu-DOTA-knottin 2.5F. The biodistribution of knottin 2.5F in healthy mice (N = 5) 1 hour post-injection. Uptake expressed as %ID/g (left) and %ID/cm^3 (right); error bars, SEM.

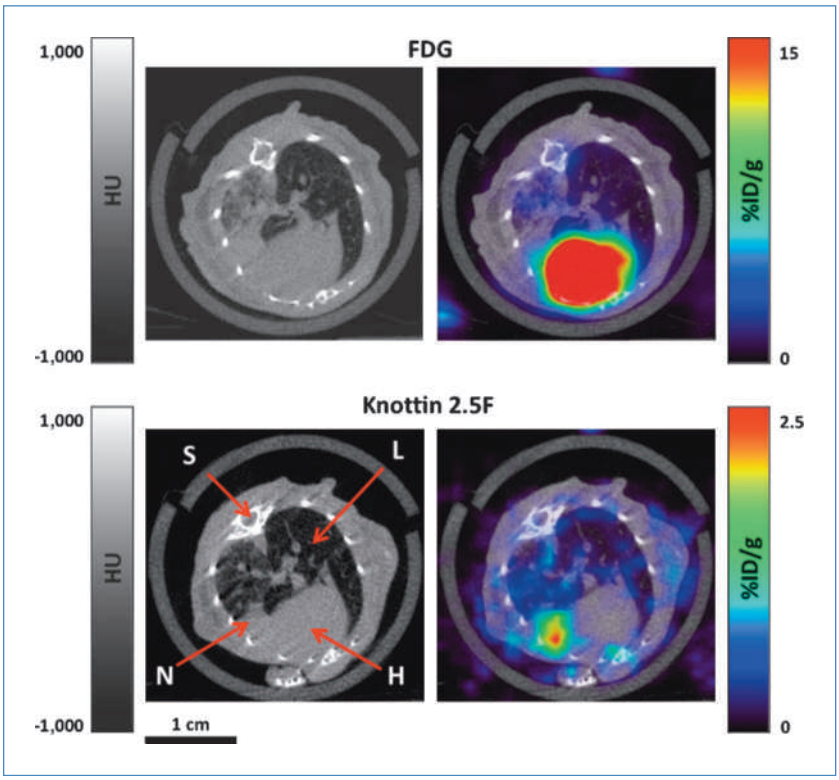

Figure 3. Small animal PET/CT. Transverse sections of the same mouse imaged with FDG (top) and knottin 2.5F (bottom). Left, CT images showing the lungs (L), heart (H), spine (S), and a nodule (N) immediately adjacent to the heart. Gray scale, Hounsfield units (HU). Right, fused PET/CT images. The nodule can easily be outlined based on the knottin 2.5F, whereas the high uptake of FDG in the heart makes it difficult to delineate the nodule. Note different maximum values on top and bottom PET color scale bars.

$P < 0.05$ by two-sided Mann-Whitney test; Fig. 4). Higher tumor-to-background ratios of ^{64}Cu-DOTA-knottin 2.5F result from low background in the thorax, which facilitates nodule identification in regions made inaccessible by higher background ^{18}F-FDG uptake (0.30 ± 0.03%ID/g for ^{64}Cu-DOTA-knottin 2.5F versus 1.35 ± 0.13%ID/g for FDG; Fig. 5 and Supplementary Fig. S2).

Immunofluorescence

Mouse lung with nodules identified with ^{64}Cu-DOTA-knottin 2.5F PET were double-stained for mouse CD31, a marker expressed on endothelial cells, and α_v-integrin subunit to confirm the presence of the imaging target. Immunofluorescence showed colocalization of CD31 and α_v, (Fig. 5), which confirms the presence of the imaging target on the tumor vasculature.

Discussion

Despite advances in diagnostic clinical imaging, there is a critical need for new imaging agents and new methods that allow noninvasive characterization of lung lesions in the subcentimeter range. Engineered knottin peptides have recently been validated by our group to specifically image integrin-expressing tumors in xenograft mouse models (17, 19, 24–27). Here we expand on our previous work and show that we can characterize spontaneous lung tumors developing in a conditional transgenic mouse model with the use of ^{64}Cu-DOTA-knottin 2.5F and combined small animal PET/CT. These transgenic mouse models provide a unique opportunity to study tumorigenesis in a lung cancer model that more closely resembles the "natural" development and progression of human cancer. Because there is always an underlying concern with the use of artificial xenografts

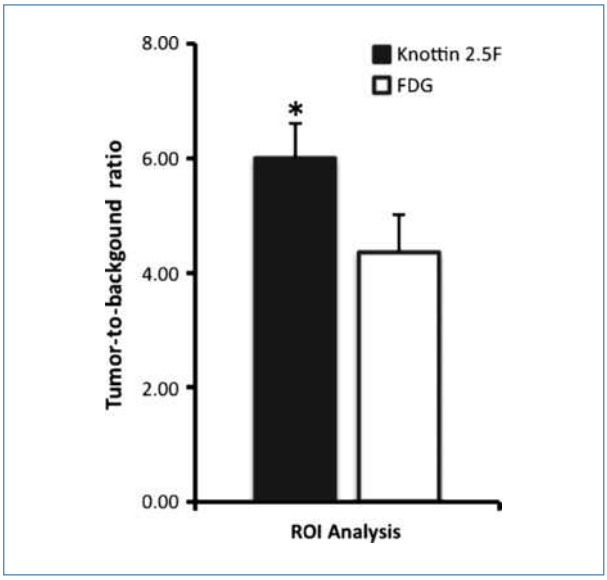

Figure 4. Tumor-to-background ratio of knottin 2.5F and FDG. ROIs were drawn over tumors ($N = 10$) and areas in the lungs without visible tumor mass on CT (background). For each ROI the mean uptake in %ID/g was estimated and the tumor-to-background ratio calculated. Bars, mean ± SEM. *, $P < 0.05$ for two-sided Mann-Whitney test.

Table 1. Results of quantitative ROI analysis

Tumor No.	Uptake (%ID/g)		Tumor-to-background	
	Knottin 2.5F	FDG	Knottin 2.5F	FDG
1	2.36	14.9	7.44	8.30
2	1.65	5.10	5.20	2.84
3	1.30	5.10	4.10	2.84
4	1.39	7.08	4.38	3.94
5	1.75	5.33	8.29	3.67
6	2.03	4.60	7.44	5.56
7	2.12	8.72	5.71	7.36
8	1.99	5.10	9.05	4.78
9	1.38	4.46	3.51	2.64
10	1.66	2.41	4.94	1.70
$\bar{X}$	1.76	6.28	6.01	4.36
$SE_{\bar{X}}$	0.11	1.09	0.61	0.68

models (28, 29), these studies provide additional information that will aid in clinical translation of newly developed molecular imaging probes.

The performance of knottin 2.5F, a peptide engineered to target integrin receptors, was compared with that of ^{18}F-FDG. We were able to obtain a higher tumor-to-background ratio with ^{64}Cu-DOTA-knottin 2.5F compared with ^{18}F-FDG (6.01 ± 0.61 versus 4.36 ± 0.68; $P < 0.05$) due to a low background signal in the area of interest. It has previously been reported that anesthesia does not influence the tumor uptake of FDG (30). It is unlikely that the difference in tumor-to-background ratio can be addressed to the difference in anesthetic regiment between the two probes during PET imaging. Lung lesions imaged with ^{64}Cu-DOTA-knottin 2.5F are clearly visible, allowing for easier image interpretation compared with ^{18}F-FDG due to a large spillover effect from uptake in the heart. However, it is important to note that in a few cases, the quantification of ^{18}F-FDG uptake is biased toward a higher tumor uptake because of this spillover from the heart to the adjacent lung tumors. The presence of the α_v-integrin imaging target on the tumor neovasculature was confirmed by *ex vivo* fluorescence microscopy. Furthermore, in a previous study we determined the specificity of integrin-binding knottin probes by competition with an excess of unlabeled peptide (19). Collectively, our results indicate that engineered knottin peptides are able to provide detailed molecular information about receptors expressed on vascular endothelium and the surface of tumors. Studies that use dynamic PET imaging and compartment modeling are in progress to investigate the fraction of the signal originating from knottins bound to integrins on the endothelium compared with the surface of the tumor.

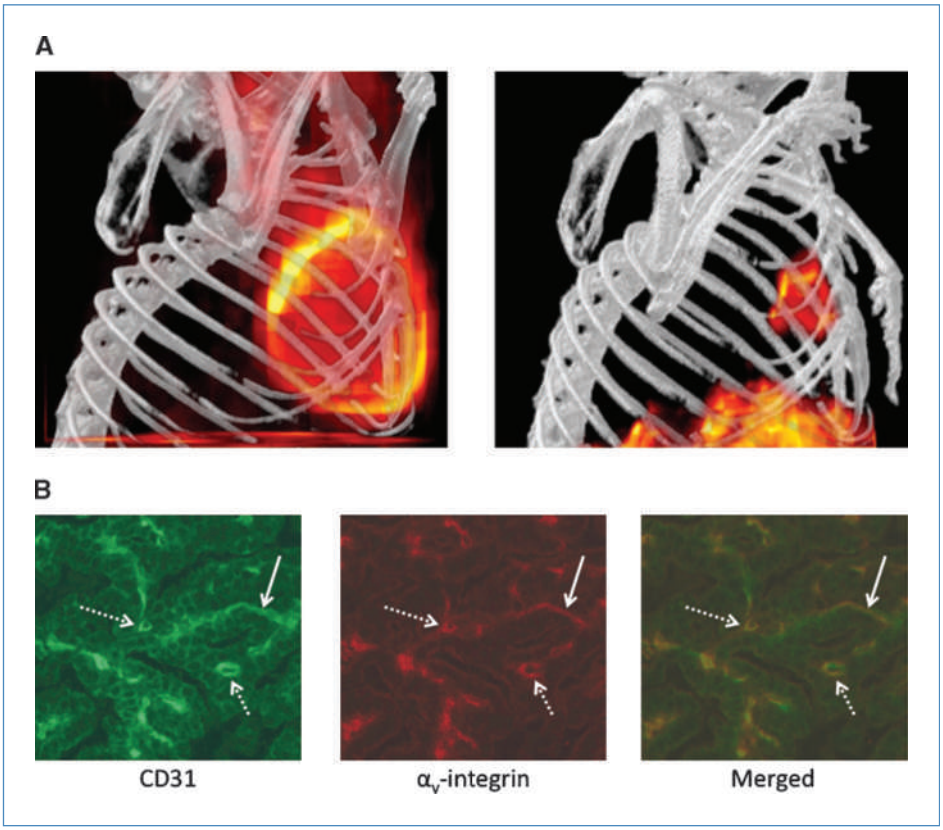

Figure 5. A, volume renderings of the thorax of a mouse imaged with FDG (left) and knottin 2.5F (right). A nodule is present immediately adjacent to the heart and is clearly visible when knottin 2.5F is used. The intense FDG uptake in the heart makes it impossible to delineate the nodule. Movies of the volume rendering images are available online as supplementary material. B, immunofluorescence of tumor sections. Sections were stained for CD31 (left) and α_v-integrin (center). Merging of the two images (right) shows that the expression of α_v-integrin colocalizes with the expression of the CD31 on the vessels (arrows).

Clinical studies with radiolabeled RGD peptides (^{18}F-galacto-RGD and ^{18}F-AH111585) for PET imaging have shown the feasibility of imaging integrin receptors expressed on tumor cells and tumor neovasculature in cancer patients (17, 31–35). In addition, recent studies show that the pharmacokinetics of integrin-targeting peptides may easily be fine-tuned (19, 36, 37). For example, in an orthotopic lung cancer mouse model, PET imaging with ^{64}Cu-DOTA–labeled PEGylated dimeric cyclic RGD peptide showed better tumor delineation compared with imaging with ^{18}F-FDG. These studies show the potential of integrin imaging for early diagnosis and primary staging of lung cancer (15).

An important characteristic of any imaging probe is its uptake efficiency at the tumor site and its lack of accumulation at nontumor sites. The optimal probe will have high affinity for the target of interest, leading to high uptake, and at the same time show minimal background accumulation (38). Significant work has been put into engineering multimeric RDG peptide probes with increased affinity toward integrins. Multimeric RGD peptide probes show higher tumor accumulation and retention *in vivo*, but are also accompanied by and increase uptake in nontumor tissues (36, 39, 40). In contrast, engineering of the knottin scaffold with the monomeric RGD binding motif shows comparable affinity toward integrins as the tetrameric RGD peptide ^{64}Cu-DOTA-E{E[c(RGDfK)]$_2$}$_2$ while maintaining a low accumulation in normal tissues, leading to a higher tumor-to-nontumor tissue ratio (Supplementary Table S1).

A common criterion for diagnosing malignancy with FDG-PET clinically is the standardized uptake value, which is a measure of the absolute uptake in a given region normalized for injected dose and body mass. However, it has been reported that using the tumor-to-background ratio improves the sensitivity of FDG-PET for diagnosis of small pulmonary nodules (7). In the current study, the absolute radiotracer uptake in the lung tumors was higher for FDG than for knottin 2.5F. This example shows that the comparatively better contrast shown by knottin 2.5F was due to lower background signal in the thorax for ^{64}Cu-DOTA-knottin 2.5F compared with ^{18}F-FDG. Together, the favorable biodistribution and tumor accumulation merit further investigation to see if these findings translate to the clinical setting.

Knottins have previously been shown to be nonimmunogenic, and a synthetic version of the knottin MVIIA (Ziconotide) is approved for treatment of chronic pain (19, 41). We have successfully done up to six imaging sessions over 8 months with ^{64}Cu-DOTA-knottin 2.5F in immunocompetent mice without the observation of an acute immune response (data not shown). This shows that repeated imaging with ^{64}Cu-DOTA-knottin 2.5F in mice is possible. However, rigorous toxicity studies will be required before clinical translation to minimize the possibility of an unexpected immunologic reaction against ^{64}Cu-DOTA-knottin 2.5F.

The transgenic mouse model allows us to investigate if imaging of integrin expression with ^{64}Cu-DOTA-knottin 2.5F can be used to characterize the lesions identified on CT as malignant. However, the difficulties of generating adequate numbers of transgenic mice with the right genotype and the inability to control the exact latency of tumor development after administration of doxycycline made a rigorous investigation of the tumor development at the earliest time impossible. Therefore, we were not able to investigate in detail the minimal detectable size of lung nodules that can be characterized as malignant by integrin imaging, but based on our data we were able to characterize nodules as small as 3 mm in diameter as malignant (Fig. 3). Some of the mice (N = 2) had lesions <3 mm in diameter visible on CT (N = 5). ^{64}Cu-DOTA-knottin 2.5F was able to delineate one lesion with a diameter of 2.5 mm but missed the other small lesions, whereas FDG missed all of the lesions <3 mm in diameter. Assuming that all lesions detected by CT are true-positive findings, the sensitivity of ^{64}Cu-DOTA-knottin 2.5F and FDG for all lesions is 73.3% and 66.7% respectively, and 100% for both probes for lesions >3 mm in diameter. Although we do not have histology to confirm the malignancy of the smaller lesions, we know from previous work that lung lesions detected by CT correspond with lung cancer (20). A possible explanation for failed detection of those small lesions by PET could be loss of contrast in the PET images due to blurring originating from respiratory motion during the PET acquisitions and partial volume effect. Unlike CT, no respiratory gating was applied during the PET acquisitions.

Because of the relative poor resolution of clinical PET scanners the partial volume effect becomes substantial for tumors in the subcentimeter range. For small tumors, partial volume effect will lead to underestimation of the true uptake and decreased sensitivity; however, with the use of mathematical models, it is possible to correct for partial volume effect. With a combination of morphologic information obtained from CT images, correction for respiratory motion, and low background signal from engineered peptides, such as ^{64}Cu-DOTA-knottin 2.5F, partial volume effect–corrective algorithms will likely lead to better estimations of true uptake in lung nodules (42). Furthermore, clinical scanners with improved spatial resolution continue to be developed, which, if married to the right tracers, have significant potential for improved cancer diagnostics/management.

The clinical utility of ^{64}Cu-DOTA-knottin 2.5F imaging will have to be carefully studied in patients with different types of lung cancer. If knottin 2.5F imaging is able to outperform FDG, it could replace FDG-PET. Alternatively, if the knottin 2.5F imaging agent is not able to do as well as FDG, then it could be used in cases in which FDG uptake is borderline, as indicated by an intermediate standardized uptake value. In these cases, FDG is unable to distinguish inflammation versus tumor, and the knottin 2.5F may help to do so.

In summary, our results show that engineered peptides, such as ^{64}Cu-DOTA-knottin 2.5F, have the potential to be used in early detection of lung cancer. However, further studies are needed to address the smallest detectable tumor size by ^{64}Cu-DOTA-knottin 2.5F. Further studies will also be needed to understand ^{64}Cu-DOTA-knottin 2.5F uptake in sites of pulmonary infection and inflammation, which could lead to upregulation of integrins during the inflammatory process. Together with improvements in scanner spatial resolution/sensitivity, partial volume effect correction, and further engineering of knottins to

improve the tracer performance, PET imaging with engineered knottins might prove to be more sensitive than FDG-PET for primary diagnosis of lung lesions.

Disclosure of Potential Conflicts of Interest

No potential conflicts of interest were disclosed.

Acknowledgments

We thank Pauline Chu for her kind help with tissue staining, the Stanford University Cyclotron and Radiochemistry Facility for synthesis of ^{18}F-FDG, and Dr. Zhe Liu for his help with ^{64}Cu radiolabeling of the knottin peptide.

Grant Support

NIH grants National Cancer Institute In Vivo Cellular and Molecular Imaging Center P50 CA114747 and Center of Cancer Nanotechnology Excellence U54 CA119367, and the Canary Foundation (S.S. Gambhir); and the Lundbeck Foundation, the Denmark American Foundation, BioCampus University of Copenhagen, the Department of Clinical Physiology, Nuclear Medicine and PET at Rigshospitalet, and the Danish National Advanced Technology Foundation (C.H. Nielsen).

The costs of publication of this article were defrayed in part by the payment of page charges. This article must therefore be hereby marked *advertisement* in accordance with 18 U.S.C. Section 1734 solely to indicate this fact.

Received 04/20/2010; revised 09/02/2010; accepted 09/02/2010; published OnlineFirst 11/09/2010.

References

1. Sato M, Shames DS, Gazdar AF, Minna JD. A translational view of the molecular pathogenesis of lung cancer. J Thorac Oncol 2007;2:327–43.
2. Dibble R, Langeburg W, Bair S, Ward J, Akerley W. Natual history of non-small cell lung cancer in non-smokers. J Clin Oncol (Meeting Abstracts) 2005;23:7252.
3. Henschke CI, Yankelevitz DF, Libby DM, Pasmantier MW, Smith JP, Miettinen OS. Survival of patients with stage I lung cancer detected on CT screening. N Engl J Med 2006;355:1763–71.
4. Wang T, Nelson RA, Bogardus A, Jr., FWG. Five-year lung cancer survival. Cancer 2010;116:1518–25.
5. Black WC. Computed tomography screening for lung cancer: review of screening principles and update on current status. Cancer 2007;110:2370–84.
6. Giaccone G. ^{18}Fluorodeoxyglucose positron emission tomography, a standard diagnostic tool in lung cancer. J Natl Cancer Inst 2007;99:1741–3.
7. Nomori H, Watanabe K, Ohtsuka T, Naruke T, Suemasu K, Uno K. Evaluation of F-18 fluorodeoxyglucose (FDG) PET scanning for pulmonary nodules less than 3 cm in diameter, with special reference to the CT images. Lung Cancer 2004;45:19–27.
8. Gould MK, Maclean CC, Kuschner WG, Rydzak CE, Owens DK. Accuracy of positron emission tomography for diagnosis of pulmonary nodules and mass lesions: a meta-analysis. JAMA 2001;285:914–24.
9. Ung YC, Maziak DE, Vanderveen JA, et al. ^{18}Fluorodeoxyglucose positron emission tomography in the diagnosis and staging of lung cancer: a systematic review. J Natl Cancer Inst 2007;99:1753–67.
10. Murakami S, Saito H, Sakuma Y, et al. Correlation of (18)F-fluorodeoxyglucose uptake on positron emission tomography with Ki-67 index and pathological invasive area in lung adenocarcinomas 30 mm or less in size. Eur J Radiol 2010;75:e62–6.
11. Vansteenkiste JF, Stroobants SS. PET scan in lung cancer: current recommendations and innovation. J Thorac Oncol 2006;1:71–3.
12. Abe K, Baba S, Kaneko K, et al. Diagnostic and prognostic values of FDG-PET in patients with non-small cell lung cancer. Clin Imaging 2009;33:90–5.
13. Izuishi K, Kato K, Ogura T, Kinoshita T, Esumi H. Remarkable tolerance of tumor cells to nutrient deprivation: possible new biochemical target for cancer therapy. Cancer Res 2000;60:6201–7.
14. Carmeliet P, Jain RK. Angiogenesis in cancer and other diseases. Nature 2000;407:249–57.
15. Chen X, Sievers E, Hou Y, et al. Integrin αvβ3-targeted imaging of lung cancer. Neoplasia 2005;7:271–9.
16. Cai W, Gambhir SS, Chen X. Multimodality tumor imaging targeting integrin $\alpha_v\beta_3$. BioTechniques 2005;39:S14–25.
17. Kimura RH, Levin AM, Cochran FV, Cochran JR. Engineered cystine knot peptides that bind αvβ3, αvβ5, and α5β1 integrins with low-nanomolar affinity. Proteins 2009;77:359–69.
18. Kolmar H. Biological diversity and therapeutic potential of natural and engineered cystine knot miniproteins. Curr Opin Pharmacol 2009;9:608–14.
19. Kimura RH, Cheng Z, Gambhir SS, Cochran JR. Engineered knottin peptides: a new class of agents for imaging integrin expression in living subjects. Cancer Res 2009;69:2435–42.
20. Tran PT, Fan AC, Bendapudi PK, et al. Combined inactivation of MYC and K-Ras oncogenes reverses tumorigenesis in lung adenocarcinomas and lymphomas. PLoS One 2008;3:e2125.
21. Felsher DW, Bishop JM. Reversible tumorigenesis by MYC in hematopoietic lineages. Mol Cell 1999;4:199–207.
22. Knoess C, Siegel S, Smith A, et al. Performance evaluation of the microPET R4 PET scanner for rodents. Eur J Nucl Med Mol Imaging 2003;30:737–47.
23. Loening AM, Gambhir SS. AMIDE: a free software tool for multimodality medical image analysis. Mol Imaging 2003;2:131–7.
24. Willmann JK, Kimura RH, Deshpande N, Lutz AM, Cochran JR, Gambhir SS. Targeted contrast-enhanced ultrasound imaging of tumor angiogenesis with contrast microbubbles conjugated to integrin-binding knottin peptides. J Nucl Med;51:433–40.
25. Miao Z, Ren G, Liu H, et al. An engineered knottin peptide labeled with ^{18}F for PET imaging of integrin expression. Bioconjug Chem 2009;20:2342–7.
26. Jiang L, Kimura RH, Miao Z, et al. Evaluation of a (64)Cu-labeled cystine-knot peptide based on agouti-related protein for PET of tumors expressing αvβ3 integrin. J Nucl Med ;51:251–8.
27. Kimura RH, Miao Z, Cheng Z, Gambhir SS, Cochran JR. A dual-labeled knottin peptide for PET and near-infrared fluorescence imaging of integrin expression in living subjects. Bioconjug Chem 2009;20:2342–7.
28. Carver BS, Pandolfi PP. Mouse modeling in oncologic preclinical and translational research. Clin Cancer Res 2006;12:5305–11.
29. Olive KP, Tuveson DA. The use of targeted mouse models for preclinical testing of novel cancer therapeutics. Clin Cancer Res 2006;12:5277–87.
30. Fueger BJ, Czernin J, Hildebrandt I, et al. Impact of animal handling on the results of ^{18}F-FDG PET studies in mice. J Nucl Med 2006;47:999–1006.
31. Haubner R, Weber WA, Beer AJ, et al. Noninvasive visualization of the activated αvβ3 integrin in cancer patients by positron emission tomography and [^{18}F]galacto-RGD. PLoS Med 2005;2:e70.
32. Beer AJ, Grosu AL, Carlsen J, et al. [^{18}F]galacto-RGD positron emission tomography for imaging of αvβ3 expression on the neovasculature in patients with squamous cell carcinoma of the head and neck. Clin Cancer Res 2007;13:6610–6.
33. Beer AJ, Lorenzen S, Metz S, et al. Comparison of integrin αVβ3 expression and glucose metabolism in primary and metastatic

lesions in cancer patients: a PET study using ^{18}F-galacto-RGD and ^{18}F-FDG. J Nucl Med 2008;49:22–9.
34. Kenny LM, Coombes RC, Oulie I, et al. Phase I trial of the positron-emitting Arg-Gly-Asp (RGD) peptide radioligand ^{18}F-AH111585 in breast cancer patients. J Nucl Med 2008;49:879–86.
35. Schnell O, Krebs B, Carlsen J, et al. Imaging of integrin α(v)β(3) expression in patients with malignant glioma by [^{18}F] galacto-RGD positron emission tomography. Neuro Oncol 2009;11:861–70.
36. Liu S, Liu Z, Chen K, et al. (18)F-labeled galacto and PEGylated RGD dimers for PET imaging of α(v)β (3) integrin expression. Mol Imaging Biol 2010;12:530–8.
37. Wu Z, Li ZB, Chen K, et al. MicroPET of tumor integrin αvβ3 expression using ^{18}F-labeled PEGylated tetrameric RGD peptide (^{18}F-FPRGD4). J Nucl Med 2007;48:1536–44.
38. Gambhir SS. Molecular imaging of cancer with positron emission tomography. Nat Rev Cancer 2002;2:683–93.
39. Li ZB, Cai W, Cao Q, et al. (64)Cu-labeled tetrameric and octameric RGD peptides for small-animal PET of tumor α(v)β(3) integrin expression. J Nucl Med 2007;48:1162–71.
40. Wu Y, Zhang X, Xiong Z, et al. MicroPET imaging of glioma integrin $\alpha_v\beta_3$ expression using (64)Cu-labeled tetrameric RGD peptide. J Nucl Med 2005;46:1707–18.
41. Smith HS, Deer TR. Safety and efficacy of intrathecal ziconotide in the management of severe chronic pain. Ther Clin Risk Manag 2009; 5:521–34.
42. Teo BK, Seo Y, Bacharach SL, et al. Partial-volume correction in PET: validation of an iterative postreconstruction method with phantom and patient data. J Nucl Med 2007;48:802–10.